Supporting Information

Self-Amplifying Cascade Strategy Triggered Au NPs Assembly for Ultrasensitive cTnI Detection with Dynamic Light Scattering

Chen Chen[a, 1], Ying Qing Li[b, 1], Xiaosong Yang[b, *], Liansheng Ling[a, *], Ji Zhang [b, *]

[a] *School of Chemistry, Sun Yat-Sen University, Guangzhou 510006, China*

[b] *State Key Laboratory of Oncology in South China, Collaborative Innovation Center of Cancer Medicine, Sun Yat-sen University Cancer Center, Guangzhou 510006, China*

1.1 Characterization of GOD/Fe-MOF

The surface morphology of the Fe-MOF and the resulting GOD/Fe-MOF composite was characterized by SEM. As depicted in Figure S1A, the Fe-MOF exhibited cubic structures. Following the immobilization of GOD, the surface of GOD/Fe-MOF composite became rough, however retained the core morphological features of the MOF without significant structural alteration (Figure S1B), indicating successful enzyme incorporation without disrupting the framework integrity.

Further Energy-dispersive X-ray spectroscopy (EDX) quantification proved the composite synthesis. Elemental analysis of the Fe-MOF revealed the expected constituents: carbon (C), oxygen (O), and iron (Fe), with the Fe mass fraction reaching 30.14% (Figure S1C). In contrast, the EDX profile of the GOD/Fe-MOF composite showed distinct additional peaks corresponding to phosphorus (P) and sulfur (S) (Figure S1D), elements inherent to the GOD enzyme. Crucially, the composite maintained a high Fe mass fraction (20.73%), providing strong evidence for the effective doping of GOD within the MOF matrix to form the functional GOD/Fe-MOF composite.

The chemical structure of the GOD/Fe-MOF composite was further elucidated by FT-IR spectroscopy. The spectrum of the Fe-MOF (Figure S1E, curve green) displayed characteristic absorption bands corresponding to organic ligand (NH_2-BDC) and metal-

organic framework: symmetric and asymmetric COO^- stretching vibrations at 1297 cm^{-1} and 1555 cm^{-1}, respectively, and the Fe-O bond bending vibration at 770 cm^{-1}. Following GOD immobilization, the FT-IR spectrum of the GOD/Fe-MOF (curve blue) composite retained the principal MOF-associated bands, confirming framework stability post-modification. Crucially, new diagnostic peaks emerged, unequivocally signifying successful enzyme incorporation. The C-H stretching vibration from methyl and methylene groups was evident at 2930 cm^{-1}. Additional key bands included the amide I band (C=O stretch) at 1640 cm^{-1} and the amide II band (a combination of N-H bend and C-N stretch modes) at 1400 cm^{-1}, which were characteristic of the peptide backbone in GOD, and an additional band near 930 cm^{-1} were assigned to C-H bending modes. The coexistence of these GOD-specific vibrational signatures alongside the preserved MOF fingerprint bands provides compelling spectroscopic evidence for the successful formation of the GOD/Fe-MOF composite material.

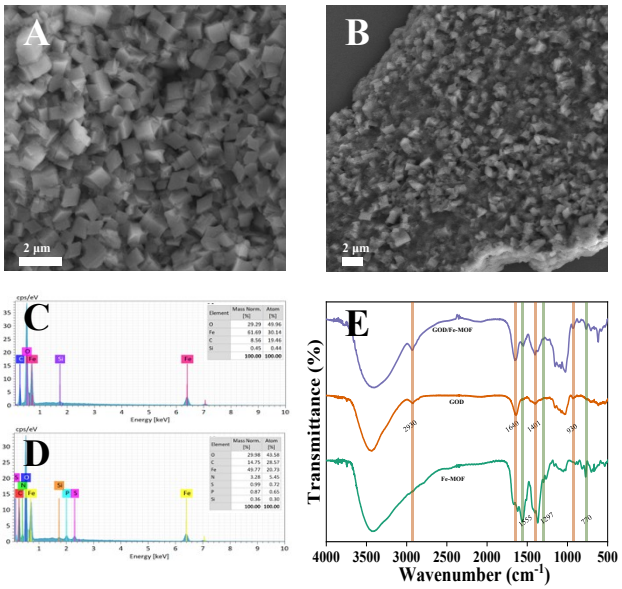

Figure S1. SEM characterization of (A) Fe-MOF, (B) GOD/Fe-MOF. EDX of Fe-MOF (C) and (D) GOD/Fe-MOF. (E) FT-IR characterization of Fe-MOF, GOD, GOD/Fe-MOF.

1.2 Exploration the acidic microenvironment

The pH of the reaction system before and after the addition of glucose was measured. As shown in Figure S2, the initial pH value of the reaction buffer was about 7.4. After glucose was added and cultured for 20 minutes, the pH value dropped to about 5.2 due to the production of gluconic acid catalyzed by GOD.[1,2] According to prior studies on Fe-MOF have shown that significant framework disintegration occur when the pH dropped below approximately 5.5, with near-complete decomposition occurring at pH 4.5–5.0.[3] Consequently, the gluconic acid generated within the sensing system not only promoted the decomposition of the Fe-MOF but also created an acidic microenvironment conducive to the Fenton reaction.

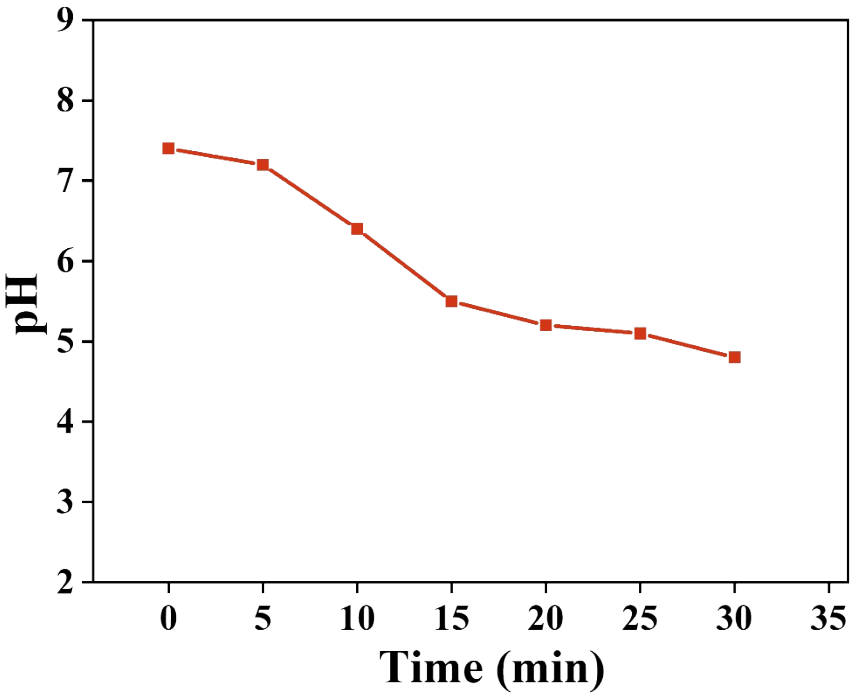

Figure S2. The change of pH value in the system.

1.3 DLS interference test and homogeneous catalysis verification

The full-range DLS (1-1000 nm) of the reaction solution was performed, both in the presence and absence of Au NPs. As shown in Figure S3A (the absence of Au NPs), the signal at 60 nm was attributed to impurities such as MOF fragments, proteins and organic ligands and a faint signal was observed above 700 nm, which could originate from a small amount of incompletely degraded MOF. In stark contrast, when Au NPs were present (Figure S3B), the DLS spectrum displayed a single and distinct peak centered at 270 nm. This indicated that the scattering contribution from impurities such as MOF fragments was negligible when the presence of aggregated-Au NPs. This observation was consequence of the intensity-weighted nature of DLS. The scattered light intensity from a particle depends not only on its physical size but also on its scattering cross-section, which is a function of both size and the refractive index contrast between the particle and the medium.[4] The particle size of the aggregated-Au NPs was significantly larger than that of other impurities, furthermore, the surface plasmon resonance properties of the Au NPs further enhance the scattering ability.[5] Thus, the aggregated-Au NPs dominated the DLS signal.

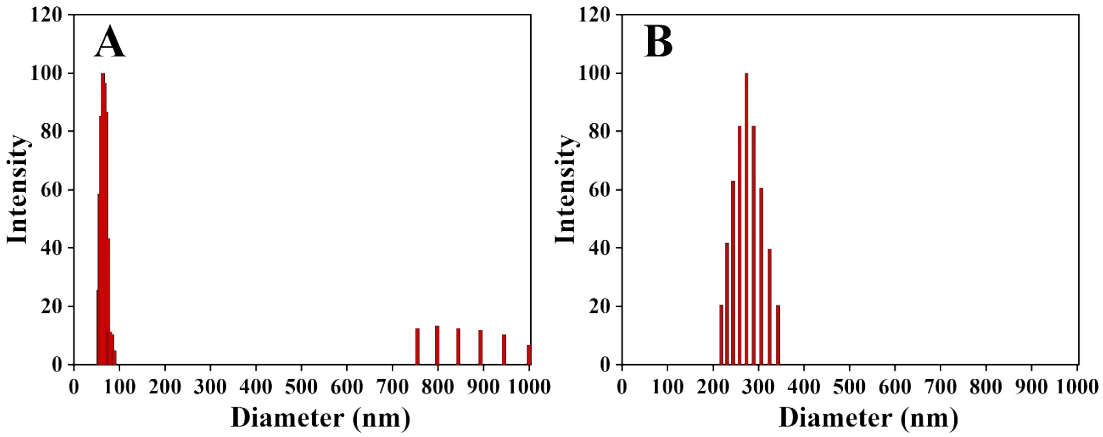

Figure S3. Full-range DLS particle size distribution diagram of Au NPs without (A) and with (B) in sensing system.

To distinguish whether the catalytic process was homogeneous (Fe^{2+} released from MOF) or heterogeneous (on intact MOF surface), the control experiment comparing systems with and without glucose was performed. As shown in the Figure S4, when glucose was absent in the system (1), gluconic acid will not be produced, the neutral

pH kept the Fe-MOF intact. Under these conditions, the DLS signal was about 30 nm, indicating that the Au NPs had hardly aggregated at all and thus virtually no catalytic activity on the intact MOF surface. However, In the presence of glucose (2), it was oxidized by GOD to form gluconic acid, and the weakly acidic pH triggered the dissociation of MOF. The released Fe^{2+} subsequently undergone a homogeneous Fenton reaction with H_2O_2 to produce •OH. This radical cleaved the DNA on the surface of Au NPs, thereby salt-induced aggregation of Au NPs generated a strong DLS signal (approximately 300 nm). This indicated that catalytic activity required the dissociation of the MOF to release Fe^{2+}, and that the intact MOF surface contributed little to this process. Therefore, this process constituted a homogeneous Fenton reaction rather than heterogeneous catalysis.

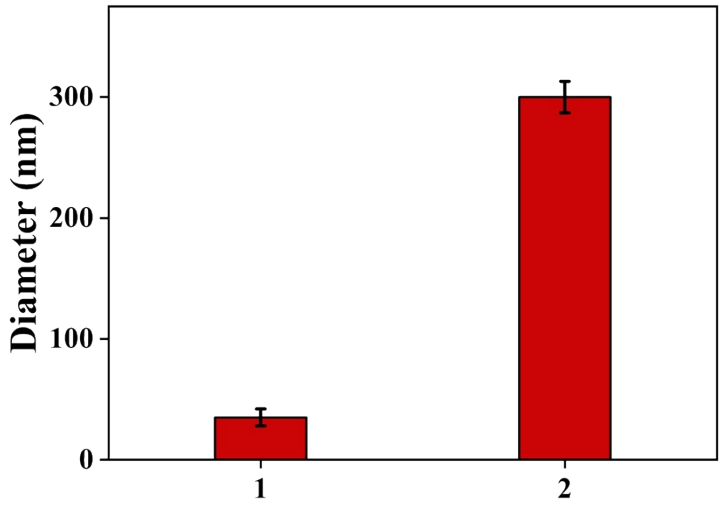

Figure S4. DLS particle size under different conditions, in the reaction system: (1) without glucose, (2) with glucose.

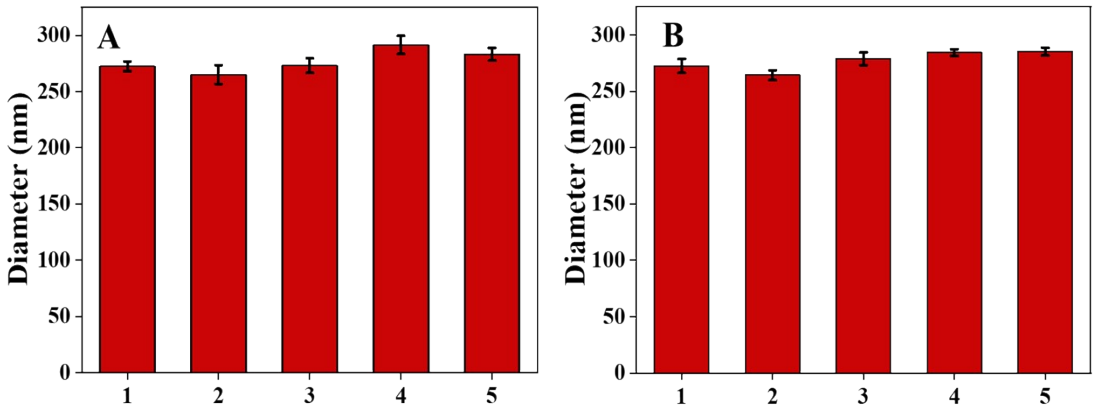

Figure S5. The investigation of (A) intra-day and (B) inter-day reproducibility of the sensor.

Table S1. Comparison of the different methods for detection of cTnI.

Methods	Target	Linear ranges (g/mL)	LODs (g/mL)	References
Potentiometric immunoassay	cTnI	1.0×10^{-11} – 1.0×10^{-8}	7.3×10^{-12}	[6]
Digital immunoassay	cTnI	0 – 5.0×10^{-9}	5.7×10^{-12}	[7]
Chemiluminescence	cTnI	1.0×10^{-11} – 5.0×10^{-8}	3.3×10^{-12}	[8]
Colorimetry	cTnI	1.0×10^{-11} – 8.0×10^{-6}	7.4×10^{-12}	[9]
Fluorescence	cTnI	8.0×10^{-10} – 2.0×10^{-7}	5.6×10^{-12}	[10]
SPR	cTnI	5.0×10^{-9} – 3.0×10^{-7}	3.6×10^{-9}	[11]
SERS	cTnI	1.0×10^{-12} – 1.0×10^{-6}	1.7×10^{-13}	[12]
LFIA	cTnI	1.0×10^{-11} – 1.5×10^{-10}	9.0×10^{-12}	[13]
Voltammetry	cTnI	5.0×10^{-11} – 5.0×10^{-10}	2.1×10^{-11}	[14]
Pressure bioassay	cTnI	1.0×10^{-11} – 1.0×10^{-8}	3.8×10^{-12}	[15]

DLS	SEA	1.0×10^{-11} – 1.0×10^{-7}	1.039×10^{-11}	[16]
DLS	Zika NS1	1.47×10^{-6} – 3.0×10^{-5}	9.6×10^{-7}	[17]
DLS	Furosemide	5.0×10^{-14} – 2.0×10^{-7}	1.96×10^{-13}	[18]
DLS	Myoglobin	1.7×10^{-12} – 1.7×10^{-8}	9.42×10^{-12}	[19]
DLS	Lactoferrin	1.5×10^{-9} – 1.5×10^{-5}	1.0×10^{-9}	[20]
DLS	AFP	6.0×10^{-11} – 5.12×10^{-7}	1.5×10^{-11}	[21]
DLS	cTnI	1.0×10^{-12} – 1.0×10^{-7}	1.5×10^{-13}	This work

Reference

[1] C. Zhang, S. Hong, M. Liu, W. Yu, M. Zhang, L. Zhang, X. Zeng and X. Zhang, *J. Control. Release*, 2020, **320**, 159-167.

[2] R. Zhao, Y. Ke, H. Sun, C. Quan, Q. Xu, J. Li, J. Guan and Y. Zhang, *Microbiol. Res*., 2025, **297**, 128149.

[3] K. Zheng, Y. Shen, J. Li, H. Zhang, Y. Dong and J. Li, *Colloid Surf. Physicochem. Eng. Asp*., 2025, **730**, 139006.

[4] Z. Jia, J. Li, L. Gao, D. Yang and A. Kanaev, *Colloids Interfaces*, 2023, **7**, 15.

[5] P. Si, N. Razmi, O. Nur, S. Solanki, C. M. Pandey, R. K. Gupta, B. D. Malhotra, M. Willander and A. de la Zerda *Nanoscale Adv*., 2021, **3**, 2679-2698.

[6] E. Ni, Y. Fang, F. Ma, G. Ge, J. Wu. Y. Wang, Y. Lin and H. Xie, *Anal. Methods*, 2020, **12**, 2914-2921.

[7] G. Zhang, L. Zhang, Y. Yu, B. Lin, Y. Wang, M. Guo and Y. Cao, *Biosens. Bioelectron*., 2020, **167**, 112502.

[8] H. Ouyang, L. Zhang, S. Jiang, W. Wang, C Zhu, Z. Fu, *Chem. Eur. J*., 2020, **26**, 7583-7588.

[9] M. Wu, X. Zhang, R. Wu, G. Wang, J. Li, Y. Chai. H and Shen, L. Li, *Anal. Lett*.,

2020, **53**, 1757-1773.

[10] J. F. Giarola, D. E. P. Souto and L. T. Kubota, *Anal. Sci*., 2021, **37**, 1007-1013.

[11] Y. Wang, Y. Yang, C. Chen, S. Wang, H. Wang, W. Jing and N. Tao, *ACS Sens*., 2020, **5**, 1126-1131.

[12] Y. Xu, Y. Zhao and Q. Jia, *Sens. Actuators. B. Chem*., 2026, **454**,139601.

[13] Z. Mirzaeizadeh, E. A. Sadrabadi, N. Naseri, H. Golmohammadi and K. OmidfarSmart, *Mater. Adv*., 2025, **6**, 839-848.

[14] A. M. Yehia, M. A. Tantawy, M. A. Farag and N. A. Abdelshafi, *Talanta*, 2025, **297**, 128661.

[15] G. Guo, X. Ren, X. Li, X. W.u, C. Qu, W. Duan and J. Zeng, *Talanta*, 2025, **289**, 127772.

[16] W. Tong, Y. Du, M. Yao, H. Fang, W. He, Y. Zhang, Y. Su, Y. Leng. X. Huang, Y. Xiong and Y. Xiong, *Food Chem*., 2025, **479**, 143713.

[17] D. L. D'Amato, I. A. A. Bessa, A. B. C. Souza, L. M. Monteiro, R. M. Borges, D. Allonso, C. B. P. Ligiero and C. M. Ronconi, *Chem. Asian J*., 2024, **19**, e202400826.

[18] H. Fang, H. Chen, Q. Guo, S. Xiong, M. Yao, X. Li, X. Huang and Y. Xiong, *Food Chem*., 2025, **492**, 145367.

[19] T. Mahatnirunkul, D. C. Tomlinson, M. J. McPherson and P. A. Millner, *Sens. Actuators. B. Chem*., 2022, **361**, 131709.

[20] K. Zhu, H. Zou, J. Chen, J. Hu, S. Xiong, J. Fu, J. Fu, Y. Xiong and X. Huang, *Food Chem*., 2023, **405**, 134983.

[21] L. Ding, J. Hu, X. Liu, J. Zeng, Z. Hu, J. Chen, K, Zhu, H. Duan and X. Huang, *Microchim. Acta*, 2024, **191**, 387.